Flat Bands Under Correlated Perturbations

Joshua D. Bodyfelt,[1] Daniel Leykam,[2] Carlo Danieli,[1] Xiaoquan Yu,[1] and Sergej Flach[1]

[1]*New Zealand Institute for Advanced Study, Centre for Theoretical Chemistry & Physics, Massey University, Auckland, New Zealand*
[2]*Nonlinear Physics Centre, Research School of Physics and Engineering, The Australian National University, Canberra ACT 0200, Australia*

Flat band networks are characterized by coexistence of dispersive and flat bands. Flat bands (FB) are generated by compact localized eigenstates (CLS) with local network symmetries, based on destructive interference. Correlated disorder and quasiperiodic potentials hybridize CLS without additional renormalization, yet with surprising consequences: (i) states are expelled from the FB energy E_{FB}, (ii) the localization length of eigenstates vanishes as $\xi \sim 1/\ln(E - E_{\rm FB})$, (iii) the density of states diverges logarithmically (particle-hole symmetry) and algebraically (no particle-hole symmetry), (iv) mobility edge curves show algebraic singularities at E_{FB}. Our analytical results are based on perturbative expansions of the CLS, and supported by numerical data in one and two lattice dimensions.

PACS numbers: 05.50.+q, 71.23.An, 71.30.+h

arXiv:1407.8345v3 [cond-mat.dis-nn] 3 Nov 2014

Introduction — Disorder has a profound effect on waves in periodic potentials, smoothing out van Hove singularities in the density of states and generating Anderson localization [1–3]. Three dimensional disordered lattices support metal-insulator transitions and mobility edges, while in one and two dimensions the effect of disorder is much simpler, localizing all eigenstates and completely suppressing transport. Correlated disorder changes this picture and allows for complex behavior even in one dimension [4]. Examples include the appearance of resonant transmission channels (random dimer model [5] and tight binding models of DNA [6, 7]), metal-insulator transitions (Aubry-André model [8]), and mobility edges (correlations with power law decay [9, 10]). Counterintuitively, certain correlations can even enhance localization [11]. Recent advances have allowed the direct observation of these fundamental effects using cold atoms [12–15] and photonic systems [16–18].

The above elastic potential scattering effects can be both strongly amplified and qualitatively changed when the kinetic energy is quenched, such as in a strictly flat dispersion band [19–24]. Flat (macroscopically degenerate) bands occur when perfect destructive interference allows for compact localized eigenstates (CLS), modes with nonzero amplitude only at a finite number of lattice sites. There are flexible approaches to designing flat band (FB) lattices in a variety of dimensions [14, 21, 25, 26], which can support new topological phases [19], and even model the fractional quantum Hall effect resulting from flat-band (FB) degeneracies of electronic Landau levels interacting within a magnetic field [20].

Anderson localization in flat bands displays a variety of unconventional features including inverse Anderson transitions [25, 27], multifractality at weak disorder [28], and effective heavy-tailed disorder distributions [29]. Recently the local symmetries of the CLS were used to detangle uncorrelated disorder into two distinct terms: one that renormalizes the energies of the CLS, and another that hybridizes them with modes belonging to other dispersive bands [30]. This detangling suggests a way to independently control the two terms using appropriately correlated potentials. Such control is feasible with ultracold atoms [12–15] and photonic systems [16–18], but can be also expected for electric or sound propagation along crystal surfaces exposed to adsorbing atoms and molecules.

In this letter, we consider locally correlated disorder and quasiperiodic potentials in flat band lattices. The compact flat band states hybridize with other dispersive degrees of freedom, but their (bare) energies are not renormalized. This leads to a strong competition between the macroscopic number of compact localized states, generating new spectral singularities (in contrast to uncorrelated disorder, which smooths out all singularities). The resulting surprising action of the perturbations is that: (i) all states are expelled from the FB energy E_{FB}, (ii) the localization length of eigenstates vanishes as $\xi \sim 1/\ln(E - E_{\rm FB})$, (iii) the density of states diverges logarithmically (particle-hole symmetry) and algebraically (no particle-hole symmetry) for disorder potentials, (iv) and metal-insulator transitions induced by quasiperiodic potentials are promoted by the flat band to mobility edges, whose curves show algebraic singularities at E_{FB}. Thus, correlated potentials provide a way to "fine-tune" the flat band singularity strength, or convert it into more useful form (e.g. mobility edge). Our analytical results are based on perturbative expansions of the CLS and supported by numerical data.

1D Model — To illustrate the idea we will start with the simplest case of a one-dimensional FB model with exactly one dispersive band and one flat band. The cross-stitch lattice, shown in the left plot in Fig.1, consists of two interconnected chains. Its unit cell is given by two lattice sites shaded in the figure, and the wave amplitude

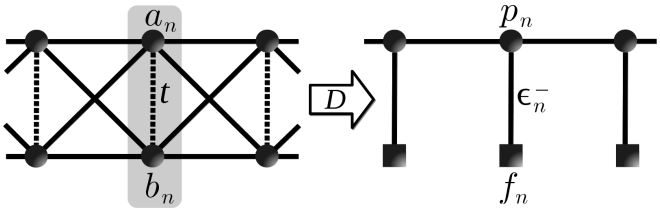

FIG. 1: The cross-stitch lattice structure (left) of Eq.(1). The detangled version of Eq.(3) is shown in the right plot.

at the cell is $\psi_n = (a_n, b_n)^T$. Stationary waves follow the eigenvalue problem

$$E\psi_n = \epsilon_n\psi_n - tV\psi_n - T(\psi_{n-1} + \psi_{n+1}) \,, \qquad (1)$$

with

$$\epsilon_n = \begin{pmatrix} \epsilon_n^a & 0 \\ 0 & \epsilon_n^b \end{pmatrix} \,, \; V = \begin{pmatrix} 0 & 1 \\ 1 & 0 \end{pmatrix} \,, \; T = \begin{pmatrix} 1 & 1 \\ 1 & 1 \end{pmatrix}.$$

In the crystalline case of $\epsilon_n = 0$, Eq.(1) is put into a Bloch basis and diagonalized to give the dispersion curves

$$E(k) = -4\cos(k) - t, \quad E_{\rm FB} = t \,.$$

One band is flat and independent of k, with Bloch modes $B_n(k) = (1,-1)^T e^{ikn}/\sqrt{2}$. Due to the degeneracy, any superposition of these Bloch modes is also an eigenmode, and one can construct compact localized modes $\psi_n = (1,-1)^T\delta_{n,n_0}/\sqrt{2}$. Applying the local rotations

$$\phi_n \equiv \begin{pmatrix} p_n \\ f_n \end{pmatrix} = D\psi_n \,, \; D = \frac{1}{\sqrt{2}}\begin{pmatrix} 1 & 1 \\ 1 & -1 \end{pmatrix}. \qquad (2)$$

with $\epsilon_n^{\pm} = (\epsilon_n^a \pm \epsilon_n^b)/2$, Eq.(1) becomes [30]

$$\begin{aligned} (\overline{E} + 2t)\, p_n &= \epsilon_n^+ p_n + \epsilon_n^- f_n - 2\,(p_{n-1} + p_{n+1}) \\ \overline{E}\, f_n &= \epsilon_n^+ f_n + \epsilon_n^- p_n, \end{aligned} \qquad (3)$$

where we measure the energy deviation from E_{FB} as $\overline{E} = E - t$, and the CLS f_n are locally hybridized with the dispersive variables p_n at strength ϵ_n^-, while their energies are renormalized exclusively through nonzero ϵ_n^+ (see Fig. 1 right). Experimental realizations of the cross-stitch model can be obtained both in its original and detangled forms; the latter having a simpler geometry easily obtained using microwave resonator networks [18].

Disorder — Real systems are never perfect and experience fluctuating deviations from an ideal setup. In Ref. [30], a disorder potential was added assuming onsite energies $\epsilon_n^{a,b}$ are random uncorrelated, with a probability density function (PDF) of finite variance $\mathcal{P}(\epsilon) = 1/W$ for $|\epsilon| \le W/2$, and $\mathcal{P} = 0$ otherwise. Excluding the CLS variables f_n from Eq.(3), one obtains

$$\frac{\epsilon_n^p - \overline{E}}{2} p_n = p_{n-1} + p_{n+1} \,, \; \epsilon_n^p = \epsilon_n^+ + \frac{(\epsilon_n^-)^2}{\overline{E} - \epsilon_n^+} - 2t, \qquad (4)$$

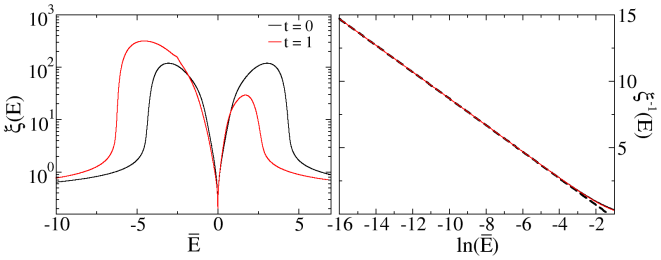

FIG. 2: Left plot: Localization length ξ versus eigenstate energy $\overline{E} = E - t$, for $t = 0$ (black solid) and $t = 1$ (red solid). Right plot: Inverse localization length ξ^{-1} versus $\ln \overline{E}$ for $\overline{E} > 0$, same color coding as in left plot. The dashed line corresponds to Eq.(6). Here, $W = 4$.

which is a tight-binding chain under an energy-dependent onsite disorder potential $z = \epsilon_n^p$. Its PDF displays Cauchy tails [30] with diverging variance at the FB energy. Consequently, at weak disorder $W \ll 1$ the localization length ξ of an eigenstate $p_n^\nu \sim e^{-\frac{n}{\xi}}$ scales as $\xi \sim 1/W^2$ away from E_{FB}, and as $\xi \sim 1/W$ at E_{FB}. This energy-dependent inverse localization length $\xi^{-1}(E)$ is numerically calculated using the recursive iteration

$$\xi^{-1}(E) = \lim_{M\to+\infty} \frac{1}{M}\sum_{n=1}^{M} \ln\left|\frac{p_{n+1}}{p_n}\right|. \qquad (5)$$

Though the disordered FB states are much more strongly localized than other states, their width still diverges for weak disorder. This is because the disorder is uncorrelated, so it performs both energy renormalization and hybridizaton with dispersive states at the same time.

A drastic change occurs when the potential is correlated such that energy renormalization no longer occurs, i.e. $\epsilon_n^a = -\epsilon_n^b$, which leads to $\epsilon_n^+ = 0$ (easily implemented with microwave resonator networks [18]). The remaining potential ϵ_n^- has PDF $\mathcal{P}(\epsilon)$, and Eq.(4) now displays a Fano resonance at energy $\overline{E} = 0$ at every lattice site, which strongly scatters the dispersive degree of freedom p_n. For small $\overline{E}$ we can neglect nonresonant terms, and substituting [31] into Eq.(5), obtain the localization length

$$\xi^{-1} = \ln\frac{W^2}{8|\overline{E}|} - 2. \qquad (6)$$

Hence irrespective of the strength W of the correlated disorder, the localization length vanishes due to resonant scattering as the energy tends towards E_{FB}. We compute the localization length numerically using Eq.(5). The results in Fig. 2 (black lines) agree excellently with the analytical predictions (dashed line).

While this picture of a macroscopic number of Fano resonances at $\overline{E} = 0$ can intuitively explain the behavior of the localization length, surprisingly the flat band energy E_{FB} is completely emptied: no eigenstate can

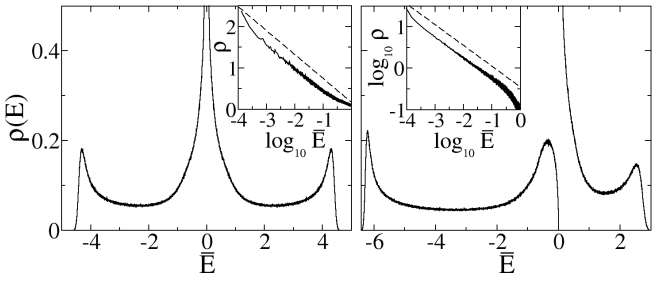

FIG. 3: Density of states $\rho(\overline{E})$ for $t = 0$ (left) and $t = 1$ (right). Divergences are observed at the flat band energies $\overline{E} = 0$. Logarithmic scalings of positive $\overline{E}$ in the insets describe the divergent behavior, and the dashed lines indicate theoretical results of Eqs. (7,8). Here, $W = 4$.

reside there. This follows directly from Eq.(3), which now allows only for a trivial solution $p_n = f_n = 0$ when $E = E_{FB} = t$. All the compact localized states have hybridized and shifted their energies away; however a significant fraction stay energetically close to E_{FB}, such that the density of states still diverges at E_{FB}. To show this, we note that close to resonance the eigenmodes should strongly excite the CLS, which may hybridize among themselves. The weak energy shifts of these states imply the existence of a small parameter, which can be used for perturbative calculations. We consider first $t = 0$. Up to normalization, we construct [31] dimer-like states at energy $\overline{E} = \pm(\epsilon_0^- \epsilon_1^-)/2 \ll W^2/4$ (position shifts can be done without loss of generality) as $f_0 = f_1 = \pm 1$, $p_0 = \pm\epsilon_1^-/2, p_1 = \epsilon_0^-/2$, $p_{n\geq 2} = \pm\epsilon_0^-(2\overline{E})^{n-1}/(\Pi_{m=2}^n \epsilon_m^-)^2$, $f_{n\geq 2} = \pm 2p_{n-1}/\epsilon_n^-$.

The density of states $\rho(\overline{E})$ for small $\overline{E}$ follows [31] from the PDF $\int_{-\infty}^{+\infty} \mathcal{P}(x)\mathcal{P}(\frac{z}{x})|x|^{-1}dx$ of the random number $z = \epsilon_0\epsilon_1$ as

$$\rho(\overline{E}) = \frac{4}{W^2}\left(\ln\frac{W}{2} - \ln\frac{4|\overline{E}|}{W}\right) . \tag{7}$$

Despite the result that eigenstates strictly do not exist at E_{FB}, the density of states $\rho(\overline{E})$ diverges logarithmically at E_{FB}.

We perform diagonalizations of Eq.(1) and obtain the density of states following well-known schemes (see chapter 3 in Ref. [32]). The result in the left of Fig. 3 confirms the predicted logarithmic divergence. It therefore also confirms that we identified the correct group of eigenstates responsible for the divergence.

When the FB energy is shifted away from the particle-hole symmetry point $E_{FB} = t \neq 0$, the nature of the localized states changes. At the energy $\overline{E} = \epsilon_0^2/(2t)$ we obtain [31] states with $f_0 = 1$, $p_0 = \epsilon_0/(2t)$, $p_{n\geq 1} = p_0(2\overline{E})^n/(\Pi_{m=1}^n \epsilon_m)^2$, $f_{n\geq 1} = 2p_{n-1}/\epsilon_n$. The dimers are destroyed, leaving single-peaked resonant states. While the localization length of these states follows the $t = 0$ case of Eq.(6) (Fig.2 red curves), the density of states behaves quite differently. First we note that the obtained states have positive $\overline{E}$, which means that they must occur on the larger energy side of the FB energy. Furthermore, the density of states $\rho(E)$ follows [31] from the PDF $f(z) = 1/(W\sqrt{z})$ of the random number $z = \epsilon_0^2$ as

$$\rho(\overline{E}) = \frac{1}{W}\sqrt{\frac{2t}{\overline{E}}} . \tag{8}$$

The divergence is now strengthened to a square root one, but only on the high energy side of the FB energy. In Fig. 3, we indeed confirm this singularity numerically on the right hand side of the FB energy. Meanwhile on the left hand side, we instead observe a vanishing density of states. It should be also noted that we observe a gap developing as t increases beyond a critical t_c [33]. This issue warrants further investigation, and may be related to disorder-induced crossing resonances [34].

Mobility edges — Since the localization length is forced to vanish at the FB energy by correlated disorder in a one-dimensional system, it can be expected that a system with a metal-insulator transition will even have a singularity in the mobility edge, i.e. the dependence of the critical potential strength on the eigenstate energy. Mobility edges typically appear for three-dimensional disordered systems, however a quasiperiodic potential is known to produce a metal-insulator transition already in one space dimension. Indeed, a tight-binding chain with eigenvalue problem $E\phi_n = \lambda\cos(2\pi\alpha n + \beta)\phi_n - (\phi_{n+1} + \phi_{n-1})$ is the well-known Aubry-André model which has a metal-insulator transition at $\lambda_c = 2$, provided α is an irrational number [8]. Note that λ_c does not depend on the eigenenergy, therefore the mobility edge function is a constant in the Aubry-André case. In general, deviations from the Aubry-André quasiperiodic case into other quasiperiodic potentials will lead to the appearance of mobility edges [35–38] - however, here we engineer them via a predictable analytical expression.

We again consider a correlated, quasiperiodic potential $\epsilon_n^a = -\epsilon_n^b = \lambda\cos(2\pi\alpha n)$. Eq.(4) can be rewritten as

$$\widetilde{E}\, p_n = \widetilde{\lambda}\cos(4\pi\alpha n)\, p_n - (p_{n-1} + p_{n+1}), \tag{9}$$

where

$$\widetilde{\lambda} = \frac{\lambda^2}{4(E-t)}, \quad \widetilde{E} := \frac{E+t}{2} - \frac{\lambda^2}{4(E-t)}. \tag{10}$$

Eq.(9) takes the form of a regular Aubry-André model, however with effective energy $\widetilde{E}$ and potential strength $\widetilde{\lambda}$, which are functions of the eigenstate energy E and the original potential strength λ, i.e. Eq.(10). Therefore if present, a metal-insulator transition must occur for $\widetilde{\lambda} = 2$. This immediately yields a mobility edge dependence $\lambda_c(E)$:

$$\left|\frac{\lambda_c^2}{4(E-t)}\right| = 2 \;\Rightarrow\; \lambda_c(E) = 2\sqrt{2|E-t|} . \tag{11}$$

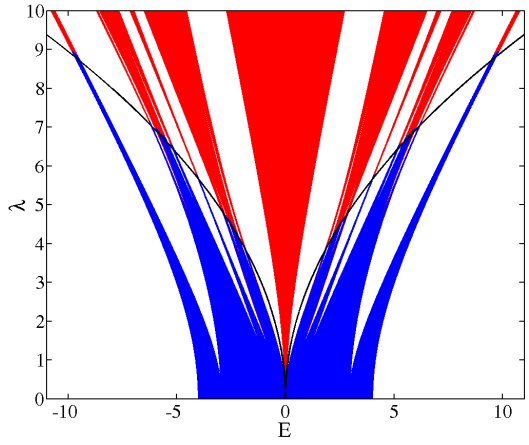

FIG. 4: Spectrum of an $N = 512$ unit cell chain under antisymmetric quasiperiodic perturbation with strength λ. The analytically predicted mobility edge Eq.(11) (black line) separates extended (blue) and localized (red; $\xi < 51$) modes.

For $E = t$, the mobility edge curve is singular and zero, corresponding to the lack of any states, as previously mentioned. In Fig. 4 we show the spectrum of Eq.(9) as a function of λ. We again compute the localization length $\xi(E, \lambda)$ with Eq.(5). If the recursion converges to a finite number (localized states, insulator), we plot blue points, while diverging cases are plotted in red (extended states, metal). The theoretical prediction Eq.(11) is also plotted and shows excellent agreement with numerical data.

Generalizations — Remarkably, this construction works in a plethora of other flat band models with CLS. In higher dimensional lattices the construction of low energy eigenstates can proceed in exactly the same way: because the localization length is forced to vanish, for sufficiently small $\overline{E}$ the eigenstates are near-sighted, so their properties are insensitive to the lattice dimension. The divergence in the density of states persists, in contrast to the more familiar van Hove singularities which get weaker as the dimension increases.

As an example, we consider the 2D Lieb lattice, which hosts a flat band with nontrivial topology. Here the compact localized states occupy multiple unit cells (shaded in Fig. 5) and form an overcomplete non-orthogonal basis. Furthermore, the flat band is frustrated: its projector is long-ranged (power law decay in real space) and it is forced to touch another dispersive band [24, 28, 39]. The band structure is determined by two dispersive $E_\pm$ and one flat E_{FB} bands [40] (here all hoppings are assumed to be of value unity):

$$E_\pm(k_x, k_y) = \pm 2\sqrt{\cos^2\frac{k_x}{2} + \cos^2\frac{k_y}{2}}\ ,\ E_{FB} = 0\ . \quad (12)$$

For a given CLS any onsite potential can be represented as a sum of a CLS-preserving part and its orthogonal counterpart. A correlated potential for that given CLS is then defined by zeroing the CLS-preserving part. Due to the above mentioned nontrivial topology of the 2D Lieb lattice, this procedure can be extended to every second CLS in a checkerboard arrangement with unit cell coordinates $l_x = m + n$ and $l_y = m - n$ (m, n are integers). We realize the correlated potential by choosing $\epsilon_{2j} = (-1)^j\delta$ in each 8-site plaquette of a participating CLS (dashed enclosure) in Fig. 5(a) (δ and the onsite energies ϵ_{2j-1} in the plaquette are random uncorrelated numbers with PDF $\mathcal{P}$). Similar to the cross-stitch example, there are rapidly decaying eigenmodes with $E \sim \delta^2 \ll W^2/2$, which yield a square root singularity in the density of states. Fig. 5(c) shows the corresponding numerical results [41]. The predicted square root singularity at $E = 0$ lies on top of a background of width W formed by the remaining CLS that have their energies renormalized. Also visible are two peaks at $E = \pm 2$, which are the van Hove singularities that have been regularized by the disorder. We note that the Lieb lattice was very recently fabricated as a photonic lattice using femtosecond laser writing [42, 43]. The required correlations can be readily introduced by modulation of the waveguide depths.

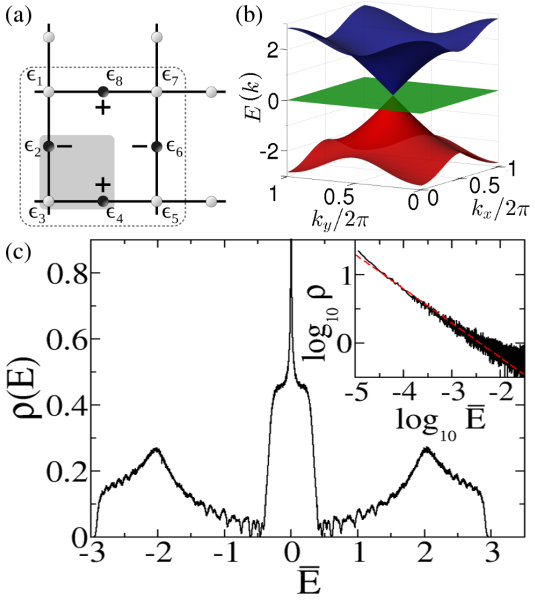

FIG. 5: (a) The 2D Lieb lattice: its unit cell (shaded region), the 8-site plaquette (dashed enclosure),and the minimal compact state (black circles). (b) The band structure $E(k_x, k_y)$ from Eq.(12). Red E_- (bottom) and blue E_+ (top) bands are dispersive, the central E_{FB} (green) band is flat. (c) Density of states under the correlation $\epsilon_{2j} = (-1)^j\epsilon_a$ enforced at each plaquette, displaying square root singularity at $E = 0$. $W = 1$. Lattice size is $N = 24 \times 24$ unit cells [44]. The red line is a linear fit.

Conclusion — We have shown how appropriately correlated disorder can transform the singular density of states at a flat band into weaker logarithmic or square root divergences. The resulting simple, analytically tractable models feature vanishing localization lengths for arbitrarily weak disorder, and mobility edges for quasiperiodic

perturbations. This approach offers a flexible and intuitive way to engineer different types of spectral singularities or mobility edges in lattice systems and control wave transport.

[1] L. Van Hove, *Phys. Rev.* **89**, 1189 (1953).
[2] P. W. Anderson, Phys. Rev. **109**, 1492 (1956).
[3] B. Kramer and A. MacKinnon, Rep. Prog. Phys. **56**, 1469 (1993).
[4] F. M. Izrailev, A. A. Krokhin, and N. M. Makarov, Phys. Rep. **512**, 125 (2012).
[5] D. H. Dunlap, H. L. Wu, and P. W. Phillips, Phys. Rev. Lett. **65**, 88 (1990).
[6] D. Klotsa, R. A. Römer, and M. S. Turner, Biophys. J. **89**, 2187 (2005).
[7] A. A. Krokhin, V. M. K. Bagci, F. M. Izrailev, O. V. Usatenko, and Y. A. Yampol'skii, Phys. Rev. B **80**, 085420 (2009).
[8] S. Aubry, G. Andre, Ann. Israel Phys. Soc. **3**, 133 (1980).
[9] F. A. B. F. de Moura and M. L. Lyra, Phys. Rev. Lett. **81**, 3735 (1998).
[10] F. M. Izrailev and A. A. Krokhin, Phys. Rev. Lett. **82**, 4062 (1999).
[11] U. Kuhl, F. M. Izrailev, and A. A. Krokhin, Phys. Rev. Lett. **100**, 126402 (2008).
[12] J. Billy et al., Nature (London) **453**, 891 (2008); G. Roati et al., ibid **453**, 895 (2008).
[13] C. Wu, D. Bergman, L. Balents, and S. Das Sarma, Phys. Rev. Lett. **99**, 070401 (2007).
[14] M. Hyrkäs, V. Apaja and M. Manninen, Phys. Rev. A **87**, 023614 (2013).
[15] L. Sanchez-Palencia and M. Lewenstein, Nat. Phys. **6**, 87 (2010).
[16] U. Kuhl, F. M. Izrailev, A. A. Krohkin, and H.-J. Stöckmann, App. Phys. Lett. **77**, 633 (2000).
[17] O. Dietz, U. Kuhl, H.-J. Stöckmann, N. M. Makarov, and F. M. Izrailev, Phys. Rev. B **83**, 134203 (2011).
[18] M. Bellec, U. Kuhl, G. Montambaux, and F. Mortessagne, Phys. Rev. B **88**, 115437 (2013).
[19] E. J. Bergholtz and Z. Lu, Int. J. Mod. Phys. B **27**, 1330017 (2013).
[20] A. Parameswaran, R. Roy, and S. L. Sondhi, Comptes Rendus Physique, **14**, 816 (2013).
[21] O. Derzhko and J. Richter, Eur. Phys. J. B **52**, 23 (2006); O. Derzhko, J. Richter, A. Honecker, M. Maksymenko, and R. Moessner, Phys. Rev. B **81**, 014421 (2010).
[22] A. Mielke, J. Phys. A **24**, L73 (1991); **24**, 3311 (1991); **25**, 4335 (1992).
[23] H. Tasaki, Phys. Rev. Lett. **69**, 1608 (1992).
[24] D. L. Bergman, C. Wu, and L. Balents, Phys. Rev. B **78**, 125104 (2008).
[25] M. Goda, S. Nishino, and H. Matsuda, Phys. Rev. Lett. **96**, 126401 (2006).
[26] S. D. Huber and E. Altman, Phys. Rev. B **82**, 184502 (2010); D. Green, L. Santos, and C. Chamon, Phys. Rev. B **82**, 075104 (2010).
[27] S. Nishino, H. Matsuda, and M. Goda, J. Phys. Soc. Jpn. **76**, 024709 (2007).
[28] J. T. Chalker, T. S. Pickles, and P. Shukla, Phys. Rev. B **82**, 104209 (2010).
[29] D. Leykam, S. Flach, O. Bahat-Treidel, and A. S. Desyatnikov, Phys. Rev. B **88**, 224203 (2013).
[30] S. Flach, D. Leykam, J. D. Bodyfelt, P. Matthies, and A. S. Desyatnikov, Europhys. Lett. **105**, 30001 (2014); ibid, **106**, 19901 (2014).
[31] Please see Supplemental Material at [URL will be inserted by publisher] for the low-energy derivations of Eqs.(6-8) and their corresponding eigenstates.
[32] H.-J. Stöckmann, Quantum Chaos, Cambridge University Press, Cambridge, 2006.
[33] The value observed is $t_c > 1$, however in such a gap we see no indication of Lifshitz-Urbach tails signifying rare states. Since our understanding is based solely on numerics, we can not completely exclude these rare events, and therefore can not provide an exact value to t_c. Further investigation into gap development is ongoing.
[34] V. A. Ignatchenko and D. S. Polukhin, JETP **116**, 206 (2013); *ibid* **117**, 846 (2013).
[35] C. M. Soukoulis and E. N. Economou, Phys. Rev. Lett. **48**, 1043 (1982).
[36] H. Hiramoto and M. Kohmoto, Phys. Rev. B **40**, 8225 (1989).
[37] P. Zhou, X. Fu, Z. Guo and Y. Liu, Solid State Commun., **96**, 372 (1995).
[38] G. Ananthakrishna, H. Zewdie, P.K. Thakur, and F. Brouers, Prog. Cryst. Growth Ch. **34**, 113 (1997).
[39] A. A. Lopes and R. G. Dias, Phys. Rev. B **84**, 085124 (2011).
[40] M. Nita, B. Ostahie and A. Aldea, Phys. Rev. B **87**, 125428 (2013).
[41] There is no gap in this case: disorder breaks the particle-hole symmetry, but the ensemble average restores it.
[42] D. Guzmán-Silva, C. Meijá-Cortés, M. A. Bandres, M. C. Rechtsman, S. Weimann, S. Nolte, M. Segev, A. Szameit, and R. A. Vicencio, New. J. Phys. **16**, 063061 (2014).
[43] F. Diebel, D. Leykam, S. Kroesen, C. Denz and A. S. Desyatnikov, Advanced Photonics, OSA Technical Digest (online) (Optical Society of America, 2014), p. NW3A.1.
[44] Because $\xi \to 0$ at E_{FB}, this is sufficient to avoid finite size effects. We checked that increasing the lattice size does not significantly change the results.

SUPPLEMENTAL MATERIAL

This Supplemental Material presents derivations of the localization length Eq.(6), the density of states Eqs.(7,8), and the profiles of the low energy eigenstates appearing in the main text.

Localization Length — For $\epsilon_n^+ = 0$, f_n can be eliminated from the eigenmode equations Eq.(3), leaving

$$\left(\frac{(\epsilon_n^-)^2}{\overline{E}} - \overline{E} - 2t\right) p_n = 2(p_{n-1} + p_{n+1}). \tag{S1}$$

When $\overline{E} \ll W^2/4$ is small, the first term on the left hand side is resonantly enhanced and dominates. The ratio $R_n = p_{n+1}/p_n$ is approximated by

$$R_n \approx \frac{(\epsilon_n^-)^2}{2\overline{E}} - \frac{1}{R_{n-1}}, \tag{S2}$$

The decaying solution for small $\overline{E}$ is $R_{n-1}(\epsilon_n^-) \approx 2\overline{E}/(\epsilon_n^-)^2$, thus applying Eq.(5) we obtain

$$\begin{aligned}\xi^{-1} &= \lim_{M\to\infty} \frac{1}{M}\sum_{n=1}^{M} \ln\left|\frac{2\overline{E}}{(\epsilon_n^-)^2}\right|, \\ &= \langle \ln\left|\frac{2\overline{E}}{(\epsilon_n^-)^2}\right|\rangle. \end{aligned} \tag{S3}$$

ϵ_n^- are uncorrelated random variables with a uniform probability distribution function (PDF),

$$f_\epsilon(x) = \begin{cases} \frac{1}{W}, & \text{if } |x| \le \frac{W}{2} \\ 0, & \text{otherwise} \end{cases} \tag{S4}$$

thus the disorder average is

$$\begin{aligned}\xi^{-1} &= \frac{1}{W}\int_{-W/2}^{W/2} \ln\left|\frac{2\overline{E}}{x^2}\right| dx \\ &= 2 + \ln\left|\frac{8\overline{E}}{W^2}\right|, \end{aligned} \tag{S5}$$

which reproduces Eq.(6) (noting that $\overline{E}/W^2 \ll 1$ and taking ξ to be positive).

Curiously, Eq.(6) incorrectly predicts $\xi^{-1} = 0$ at $\overline{E}/W^2 = 1/(8e^2) \approx 0.02$, well within the validity of the approximation $\overline{E}/W^2 \ll 1/4$. To explain this anomaly, we note that the perturbative result Eq.(S2) is only valid when $E/(\epsilon_n^-)^2 \ll 1 \Rightarrow \epsilon_n^- \gg \sqrt{E}$. Thus, the integral in Eq.(S5) requires a finite cutoff $a \sim \sqrt{E}$

$$\xi^{-1} = \frac{2}{W}\left(\int_0^a \ln|R(x)|\, dx + \int_a^{W/2} \ln\left|\frac{2\overline{E}}{x^2}\right| dx\right), \tag{S6}$$

and we require $a \ll W/2$ for the first term to be negligible. Thus, Eq.(6) is only a good approximation under the stricter condition $\sqrt{E}/W \ll 1$, which excludes the divergence of the localization length, $\xi^{-1} = 0$, at $\sqrt{E}/W \approx 0.13$.

Density of States — To obtain the density of states Eq.(7), we evaluate the PDF of the random variable $z = \epsilon_0^-\epsilon_1^-$. The product distribution $f_z(x)$ is given by

$$\begin{aligned} f_z(x) &= \int f_\epsilon(y) f_\epsilon(x/y)\frac{1}{|y|}dy, \\ &= \frac{1}{W}\int_{-W/2}^{W/2} \frac{1}{|y|} f_\epsilon(x/y) dy, \\ &= \frac{2}{W^2}\int_{2|x|/W}^{W/2} \frac{dy}{y}, \\ &= \begin{cases} \frac{2}{W^2}\left[\ln\frac{W}{2} - \ln\frac{2|x|}{W}\right], & \text{if } |x| \le \frac{W^2}{4}, \\ 0, & \text{otherwise} \end{cases} \end{aligned} \tag{S7}$$

Eq.(7) follows by making the change of variables $E = z/2$, with $\rho(E) = 2f_z(2E)$.

Similarly, we obtain Eq.(8) from the PDF of $z = \epsilon_0^2 = g(\epsilon_0)$ via

$$f_z(x) = 2|\partial_x g^{-1}(x)| f_\epsilon(g^{-1}(x)), \tag{S8}$$

where $g^{-1}(x) = \sqrt{x}$. This yields

$$f_z(x) = \begin{cases} \frac{1}{W\sqrt{x}}, & \text{if } 0 < x < \frac{W^2}{4}, \\ 0, & \text{otherwise} \end{cases} \tag{S9}$$

which gives Eq.(8) after the change of variables $E = z/(2t)$.

By the same arguments as above, the incorrectly predicted vanishing of $\rho(\overline{E})$ at $\overline{E} = W^2/4$ occurs due to realizations of the potential outside the range of validity of the perturbative expansion, and instead the stricter condition $\sqrt{E}/W \ll 1$ is again required.

Low Energy Eigenstates — The initial conditions $f_{0,1}$ uniquely determine the eigenmode amplitude along the rest of the lattice. The eigenmode equations for sites $p_{0,1}$ read

$$\left(\frac{\epsilon_0^-}{2} - \frac{\overline{E}^2}{2\epsilon_0^-} - \frac{t\overline{E}}{\epsilon_0^-}\right) f_0 = p_{-1} + \frac{\overline{E} f_1}{\epsilon_1^-}, \tag{S10}$$

$$\left(\frac{\epsilon_1^-}{2} - \frac{\overline{E}^2}{2\epsilon_1^-} - \frac{t\overline{E}}{\epsilon_1^-}\right) f_1 = p_2 + \frac{\overline{E} f_0}{\epsilon_0^-}. \tag{S11}$$

Without loss of generality, we can set $f_0 = 1$. When $\overline{E}$ is small, from the calculation of the localization length we have $p_{-1,2} \approx 2\overline{E}\, p_{0,1}/(\epsilon_{-1,2}^-)^2 \approx 0$. Under this approximation, the above equations are solved to leading order in $\overline{E}$ to obtain, for $t = 0$,

$$\overline{E} = \pm\epsilon_0^-\epsilon_1^-/2, f_1 = \pm 1, \tag{S12}$$

and when $t \neq 0$

$$\overline{E} = \epsilon_0^2/(2t), f_1 = \epsilon_0^-/(t\epsilon_1^-), \tag{S13}$$

which yield the eigenmode profiles appearing in the main text. To verify this result we also obtained eigenstates numerically for various realizations of disorder. The small $\overline{E}$ eigenstates indeed display a single strong maximum, with energy determined by disorder potential at this maximum according to the above equations.